Title

Molecular and Electronic Structure of Dinuclear Uranium Bis-μ-Oxo Complexes with Diamond Core Structural Motifs

Journal

Journal of the American Chemical Society, 136(34)

ISSN

0002-7863

Authors

Schmidt, Anna-Corina
Heinemann, Frank W.
Lukens, Wayne W.
et al.

Publication Date

2014-08-27

Molecular and Electronic Structure of Dinuclear Uranium-di-Oxo Complexes with Diamond Core Structural Motifs

Anna-Corina Schmidt,[a] Frank W. Heinemann,[a] Wayne W. Lukens Jr.,[b]* and Karsten Meyer[a]*

[a] Friedrich-Alexander University of Erlangen-Nürnberg (FAU), Department of Chemistry and Pharmacy, In-organic Chemistry, Egerlandstr. 1, 91058 Erlangen, Germany

[b] Lawrence Berkeley National Laboratory, MS: 70A-1150, Berkeley, CA 94720, USA

KEYWORDS: bis-μ-oxo uranium complex, CO_2 activation, magnetism, electronic structure

Abstract: In a multiple bond metathesis reaction, the tacn-anchored neopentyl (nP)-substituted tris-aryloxide U^{III} complex [((^{nP,Me}ArO)$_3$tacn)U^{III}] (**1**) reacts with mesitylazide and CO_2 to form mesitylisocyanate and the dinuclear bis-μ-oxo bridged U^V/U^V complex [{((^{nP,Me}ArO)$_3$tacn)UV}$_2$(μ-O)$_2$] (**3**). This reaction proceeds via the mononuclear U^V imido intermediate [((^{nP,Me}ArO)$_3$tacn)-U^V(NMes)] (**2**), which has been synthesized and fully characterized independently. The dimeric U^V oxo species shows rich redox behaviour: Complex **3** can be reduced by one and two electrons, respectively; thus, yielding the mixed-valent $U^{IV}U^V$ bis-μ-oxo [K(crypt)][{((^{nP,Me}ArO)$_3$tacn)$U^{IV/V}$}$_2$(μ-O)$_2$] (**7**) and the U^{IV}/U^{IV} bis-μ-oxo complex K$_2$[{((^{nP,Me}ArO)$_3$tacn)U^{IV}}$_2$(μ-O)$_2$] (**6**). In addition, complex **3** can be oxidized to provide the mononuclear uranium(VI) oxo complexes [((^{nP,Me}ArO)$_3$tacn)U^{VI}(O)$_{eq}$(OTf)$_{ax}$] (**8**) and [((^{nP,Me}ArO)$_3$tacn)U^{VI}(O)eq]SbF$_6$ (**9**). The unique series of bis-μ-oxo complexes also shows notable magnetic behavior, which was investigated in detail. In order to understand possible magnetic exchange phenomena, the mononuclear terminal oxo complexes [((^{nP,Me}ArO)$_3$tacn)U^V(O)(O-pyridine)] (**4**) and [((^{nP,Me}ArO)3tacn)U^V(O)(O-NMe$_3$)] (**5**) were synthesized and fully characterized. The magnetic study revealed an unusually strong antiferromagnetic exchange coupling between the two U^V ions in **3**. Examining the 18-O labeled bis-μ-oxo-bridged dinuclear complexes **3**, **6**, and **7** allowed – for the first time – the unambiguous assignment of the vibrational signature of the [U(μ-O)$_2$U] diamond core structural motif.

Although the uranyl unit $[O=U=O]^{2+}$ is ubiquitous in uranium chemistry,[1] few terminal mono oxo uranium complexes – and even fewer with a dinuclear [U=O] motif – are reported in the literature.[2] Uranium oxo complexes with the same coordination environment but different oxidation states are particularly rare.[3] Therefore, our interests have focused on the role that the metal oxidation states play in structure, reactivity, and spectroscopic properties of a series of complexes with nearly identical core structures. From such a homologous structural series, we can draw new insights into the electronic structures and reactivity of uranium-oxo complexes, which may improve our fundamental understanding of the role *f*-orbitals play in uranium–ligand multiple bonding. While bonds in 4*f*-element complexes have generally been considered to be ionic,[4] the degree of covalency in the M–L bond of 5*f* complexes, and uranium in particular, remains an important subject of debate.[5] The greater radial extension of the 5*f* valence orbitals of the early actinides can provide increased overlap with ligand orbitals, thereby enhancing the correlated magnetic behavior between bridged metal centers within a single unit, such as the structurally and electronically interesting diamond-core, M(μ-O)$_2$M. In the series of complexes presented here, considerably different magnetic behavior is observed depending on the oxidation state. Furthermore, the interplay between strong spin-orbit coupling and a low-symmetry crystal field may result in fascinating but intrinsically difficult to rationalize electronic properties, including magnetic exchange phenomena. Magnetic superexchange, while well-investigated and understood in transition metal coordination chemistry, is receiving increasing attention in actinide coordination and organometallic chemistry.[6] Antiferromagnetic exchange interaction, for instance, has been observed for most transition metal and *f*-element compounds, and Néel temperatures (T_N, defined as the maximum in the magnetic susceptibility of an antiferromagnetically coupled system) up to 1145 K are known for transition metal oxides or alloys.[7] While transition metal complexes exhibit Néel temperatures up to 270 K,[8] only relatively small values have been observed for lanthanide and actinide complexes. This weak coupling is directly related to weak interactions and small covalent contributions to the metal – ligand bonding in *f*-element complexes. By far the highest value of T_N, 110 K, for a uranium complex was published by Cummins *et al.* in 2000, for a toluene-bridged U^{III}/U^{III} complex.[6i, 9] In a landmark publication, Andersen and Edelstein *et al.* reported a dinuclear U^V organoimide, which exhibits strong exchange coupling and a T_N of 20 K.[6e] Other U^V complexes exhibit T_N from 5 to 17 K.[6a-d, 6f, g]

We now report the synthesis of three dinuclear uranium complexes bridged by two oxo ligands, which results in a diamond-shaped [U(μ-O)$_2$U] structural motif. The principal complex, a dinuclear bis-μ-oxo bridged U^V/U^V complex [{((^{nP,Me}ArO)$_3$tacn)U^V}$_2$(μ-O)$_2$], possesses a re-markably high Néel temperature of approximately 70 K, suggesting unusually strong exchange inter-actions within the [U^V(μ-O)$_2U^V$] core. In order to understand the magnetic properties of this compound – and for comparison – mononuclear uranium(V) imido, uranium(V) and uranium(VI) oxo complexes are presented as well. These new complexes have been characterized by a combination of single-crystal X-ray diffraction, ^{1}H NMR spectroscopy, elemental analysis, mass spectrometry, cyclic voltammetry, UV/vis/NIR electronic absorption, and IR /Raman vibrational spectroscopy, including 18-O isotope labeling experiments, electron paramagnetic resonance (EPR) spectroscopy, as well as variable-temperature magnetic susceptibility.

In order to synthesize high-valent oxo and imido complexes of [((^{nP,Me}ArO)$_3$tacn)U^{III}] (**1**),[10] a solution of **1** in pyridine was treated with mesitylazide. The reaction lead to an immediate color change from red to black-brown with concomitant evolution of N_2 gas to yield the U^V imido complex [((^{nP,Me}ArO)$_3$tacn)U^V(NMes)] (**2**, Scheme 1) as analytically pure, dark-brown powder in moderate yield (42 %). The addition of pyridine-N-oxide or trimethyl-N-oxide to a solution of **1** also results in a color change to orange-yellow to give the eight-coordinate, terminal U^V oxo complexes [((^{nP,Me}ArO)$_3$tacn) U^V(O)(py-NO)] and [((^{nP,Me}ArO)$_3$ tacn)-U^V(O)(Me$_3$NO)] (**4** and **5**, Scheme 1) as analytically pure, bright yellow powders in moderate and good yields (for **4**: 45 % and **5**: 68 %). However, formation of a bis-μ-oxo complex, analogous to [{((^{Ad,Me}ArO)$_3$N)U(py-NO)}(μ-O)$_2${((^{Ad,Me}ArO)$_3$N)U}], as observed in a similar reaction with the N-anchored system [{((^{Ad,Me}ArO)$_3$N)U^{III}], was not observed.[2g]

Instead, the dinuclear U^V/U^V bis-μ-oxo complex [{((^{nP,Me}ArO)$_3$tacn)U^V}$_2$(μ-O)$_2$] (**3**) was synthesized by forming **2** *in situ* and introducing CO_2 under vigorous stirring. After cooling to −35 °C, a microcrystalline precipitate formed, was filtered off, and dried *in vacuo* to give **3** (Scheme 1) as a dark-

purple, microcrystalline solid in moderate yield (42 %). Although in poor yield, complex **3** has also been synthesized *via* reaction of **1** with SeO_2, trimethylamine N-oxide (in *n*-pentane and heat), TEMPO, and, interestingly, low concentrations of neat di-oxygen. For the dinuclear complex **3**, the ESI-MS mass spectrometry shows a single molecular peak corresponding to the dimeric $[\mathbf{3}]^+$ complex with m/z = 1902. The EI+ mass spectrometry shows the molecular peak for the dimeric compound as well. These results indicate that complex **3** exists as a dimer in both solid state and solution. Reduction of **3** in benzene with excess KC_8 results in a slow color change to green-brown and yields the doubly reduced U^{IV}/U^{IV} complex $K_2[\{((^{nP,Me}ArO)_3tacn)\,U^{IV/IV}\}_2(\mu\text{-}O)_2]$ (**6**, Scheme 1) as analytically pure, pale-green powder in excellent yield (96 %). Using only one equivalent of KC_8, in the presence of equimolar amounts of 2.2.2-cryptand dissolved in THF, results in a fast color change to yellow-brown and formation of the mixed-valent U^{IV}/U^{V} complex, namely $[K(2.2.2\text{-crypt})][\{((^{nP,Me}ArO)_3tacn)U^{V/IV}\}_2(\mu\text{-}O)_2]$ (**7**, Scheme 1). Employing this synthetic protocol, **7** was isolated as a yellow-beige powder in good yield (56 %). Interestingly, complete conversion to mixed-valent **7** can also be obtained by comproportionation of equimolar amounts of pentavalent **3** and tetravalent **6** in the presence of one equivalent of 2.2.2-cryptand. Noteworthy, the reduction of the terminal oxo complexes **4** and **5** with KC_8 – in an attempt to prepare mononuclear tetravalent oxo species – shows no reaction. In light of the stability of the dinuclear U^{IV}/U^{IV} complex **6**, as well as previous[2g, 11] isolation of U^{IV} complexes with terminal oxo ligands, this result is all the more remarkable.

Finally, attempts to synthesize the oxidized, dinuclear U^{V}/U^{VI} and U^{VI}/U^{VI} complexes with Ag-salts ($AgBAr_{F24}$, $AgBPh_4$, $AgBF_4$, $AgNTf_2$, AgI, $AgNO_2$, AgO, Ag_2O, $Ag[Al(OC(CF_3)_3)_4]$) and various other oxidizing reagents (I_2, $NOBF_4$, CuSCN, CuCN, $(NH_4)_2Ce(NO_3)_6$, Au_2S, $[NMe_2(C_{18}H_{37})_2][Au(C_3S_5)_2]$, $[Fe(Cp)_2]PF_6$, $Co(Cp)_2$, NO $[Al(OC(CF_3)_3)_4]$), incorporating weakly or even non-coordinating anions, were unsuccessful. Instead, the oxi-dation of dimeric **3** with excess silver triflate or silver hexafluoro-antimonate lead to the formation of black, monomeric, terminal U^{VI} oxo complexes, namely eight-coordinate $[((^{nP,Me}ArO)_3tacn)U^{VI}(O)(CF_3SO_3)]$ (**8**) and seven-coordinate $[((^{nP,Me}ArO)_3tacn)U^{VI}(O)][SbF_6]$ (**9**) in good to excellent yields (for **8**: 63 % and **9**: 89 %). The reaction of **3** with exactly one equivalent of AgOTf or $AgSbF_6$ results in conversion of half of the starting material to yield monomeric species **8** or **9**, respectively, whereas the rest remains as the U^{V}/U^{V} dimer. To the best of our knowledge, no dinuclear, doubly-bridged U^{V}/U^{VI} or U^{VI}/U^{VI} complexes are known except for those containing the uranyl moiety.[12]

All complexes shown in Scheme 1 have been isolated in moderate to excellent yields, and have been characterized by ^1H NMR spectroscopy, single crystal X-ray diffraction, cyclic voltammetry, UV/vis/NIR absorption, and IR vibrational spectroscopy. The electronic structure and magnetic properties have been studied by X-band EPR spectroscopy and SQUID magnetization. The purity of the bulk material has been confirmed by CHN elemental analyses, except for fluoride-containing complexes **8** and **9**, where possible formation of hazardous, volatile UF_6 precluded elemental analysis. In addition to elemental analysis, title complex **3** has been characterized by mass spectrometry and vibrational spectroscopy (Raman and IR), including its 18-O labeled isotopomer.

Chart 1. Complex formulas and numbers of new uranium complexes 2 – 9, employing the starting complex $[((^{nP,Me}ArO)_3tacn)U^{III}]$ (1).

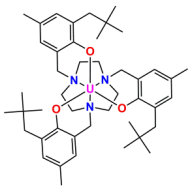

Number	Complex
1	$[((^{nP,Me}ArO)_3tacn)U^{III}]$
2	$[((^{nP,Me}ArO)_3tacn)U^{V}(NMes)]$
3	$[\{((^{nP,Me}ArO)_3tacn)U^{V}\}_2(\mu\text{-}O)_2]$
4	$[((^{nP,Me}ArO)_3tacn)U^{V}(O)(py\text{-}NO)]$
5	$[((^{nP,Me}ArO)_3tacn)U^{V}(O)(Me_3NO)]$
6	$K_2[\{((^{nP,Me}ArO)_3tacn)U^{IV/IV}\}_2(\mu\text{-}O)_2]$
7	$[K(2.2.2\text{-crypt})][\{((^{nP,Me}ArO)_3tacn)U^{V/IV}\}_2(\mu\text{-}O)_2]$
8	$[((^{nP,Me}ArO)_3tacn)U^{VI}(O)(CF_3SO_3)]$
9	$[((^{nP,Me}ArO)_3tacn)U^{VI}(O)][SbF_6]$

Scheme 1. Reaction scheme for the synthesis of complexes 2 – 9; phenolate rings, including the neopentyl and methyl substituents, are omitted for clarity.

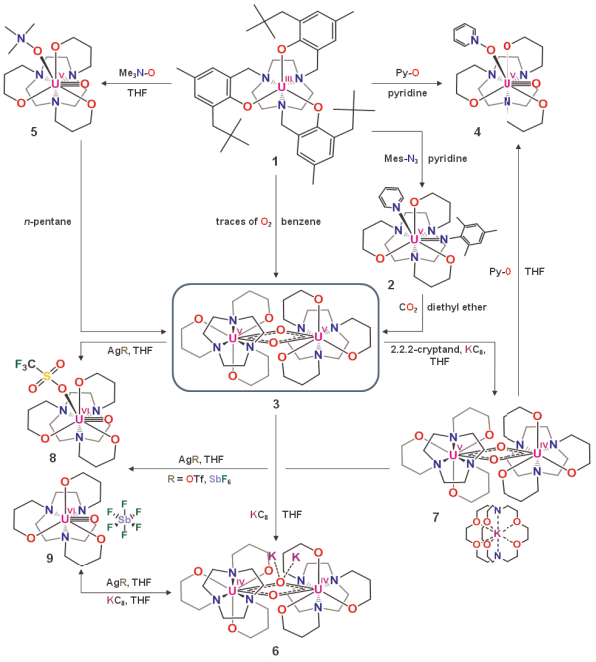

In general, the uranium ion in eight-coordinate complexes **2** – **8** is situated in a distorted trigonal dodecahedral coordination environment, with a neutral donor ligand occupying the axial position above a square plane formed by three aryloxides and the oxo/imido ligand; the uranium ion lies slightly below this square plane. The amine nitrogen atoms of the triazacyclononane (tacn) anchor form a trigonal plane opposite to the neutral donor ligand (pyridine N-oxide, trimethylamine N-oxide, pyridine). For complex **9**, the uranium ion is seven-coordinated, with a similar ligand environment as described earlier but with a free axial coordination site. In dinuclear complexes **3**, **6**, and **7**, two trigonal dodecahedral polyhedra are connected over two bridging oxygen atoms (one axial and one equatorial oxygen, see Figure 1B). While the coordination polyhedra are distorted trigonal dodecahedra, these complexes may also be viewed as *distorted octahedra* with the three amine nitrogen atoms of the tacn ligand occupying a single coordination site *trans* to the axial, neutral donor ligand, which is best illustrated in Figure 1C. The description of the coordination as distorted octahedral not only simplifies but fits the explanation of the electronic properties of these complexes (*vide infra*).

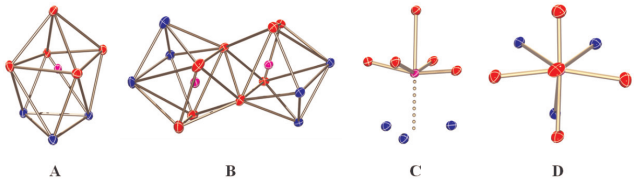

Figure 1. Trigonal dodecahedral environment for monomeric (A) and dinuclear complexes (B); Simplified distorted octahedral environment (C); View from the top (D) along the axial O–U bond, illustrating C_s symmetry for **3**, **4**, **5**, **6**, **7**, and **8** (blue: nitrogen, red: oxygen, magenta: uranium).

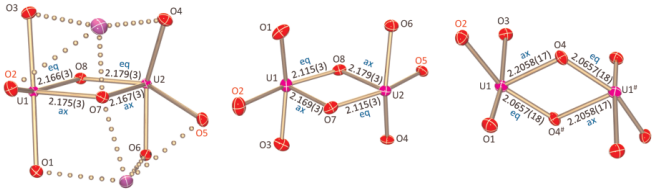

Figure 2. Diamond core structures of the dinuclear complexes **6** (left), **7** (middle), and **3** (right) with U–O bond distances. The aryloxide oxo ligands *trans* coordinated to the equatorial bridging oxo ligands are labeled in red.

Multiple bond metathesis of CO_2 with U^V imido complexes of the related adamantyl and *tert*-butyl functionalized tris(aryloxide) tacn system [(($^{R,R'}$ArO)$_3$tacn)U^V(NMes)] (with R = *t*-Bu, Ad; and R' = *t*-Bu, Me) yielded mononuclear U^V oxo complexes.[13] In these complexes, as well as in the imido precursor, the terminal, strongly π-donating oxo/imido ligand is situated on the three-fold axes of the C_3 symmetric complex.

Clearly, the most prominent structural aspect of the neopentyl-derivatized tacn system is the formation of the high-valent, dinuc-lear bis-μ-oxo bridged complex **3** with a diamond core structural motif, $[U^{V}(\mu\text{-}O)_2U^{V}]$, along with its one-elec-tron reduced mixed-valent complex $[U^{IV}(\mu\text{-}O)_2U^{V}]^{-}$ (**7**) and dou-bly-reduced $[U^{IV}(\mu\text{-}O)_2U^{IV}]^{2-}$ (**6**). In **7**, the complex anion is isolated from the encrypted potassium cation, while in **6**, both potassium ions interact with one of the two bridging oxo lig-ands. Despite of these significant structural differences, espe-cially for **6**, the metrics within the diamond core of **3**, **6**, and **7** are remarkably similar (Figure 2, Figure 3, and Table 2). In all three complexes, each bridging oxo ligand occupies an axial site on one uranium center and an equatorial site on the other. For **3** and **7**, the shorter, equatorially bound oxo is situated within the plane of the three aryloxide ligands; thus, forming a square plane with the longer, axial oxo ligand nearly perpen-dicular to this plane. For complex **6**, however, one bridging oxo is equatorial to both uranium ions, while the other bridg-ing oxo ligand, which interacts with both potassium ions, occupies the axial positions.

Complex **3** possess an inversion center in its diamond core; thus, the two equivalent uranium ions are perfectly in plane with the two bridging oxo ligands. The observed asymmetry of the U–O bond distances within the core is most distinct in $[U^{V}(\mu\text{-}O)_2U^{V}]$ with alternating short U–O_{eq} bonds at 2.066(2) Å and longer U–O_{ax} bonds at 2.206(2) Å. The core structure is further characterized by the O–U–O and U–O–U angles, which were determined to be 71.55° and 108.45°, respectively. This leads to a relatively short U···U distance of 3.422(3) Å, which compares well to the U···U separation of 3.3557(5) Å reported by Arnold and Love *et al*..[6f]

Remarkably, upon reduction, the core structural motif remains largely unperturbed. The O–U–O and U–O–U angles are all very similar at approx. 82° and 108°. While the $[U(\mu\text{-}O)_2U]$ moiety remains nearly planar (deviation from planarity: 2.23° in **6** and 0.9° in **7**), the U···U distances in these complexes show a clear trend with the degree of reduction (Table 2). Accordingly, the shortest U···U distance is found in **3** (3.422(3) Å) and the longest in doubly-reduced **6** (3.509(4) Å), while the U···U distance in mixed-valent **7** was determined to be inbetween **3** and **6** at 3.465(5) Å. As one progresses from **3** to one- and two-electron reduced **7** and **6**, the difference between short and long U–O bonds becomes less pronounced. Consequently, **6** possesses a nearly symmetric core with simi-lar U–O bond distances of 2.166(3) and 2.179(3) Å. The latter observation is particularly surprising, since two potassium cations are bound to one of the two bridging oxo ligands of **6**.

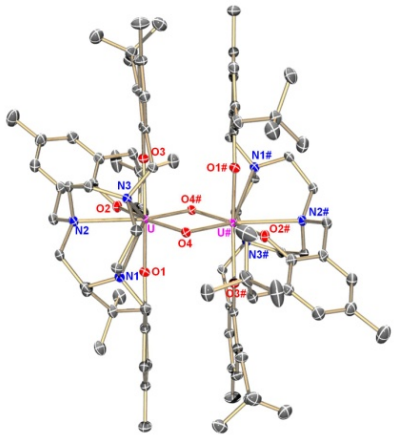

Figure 3. Molecular structures of the dinuclear uranium oxo complex: U^{V}/U^{V} **3** in crystals of **3** • 4 C_6H_6. H-atoms and co-crystallized solvent molecules are omitted for clarity. Thermal ellipsoids are at 50 % probability.

Recently, we reported the synthesis of the bis-μ-oxo bridged diuranium species [{((^{Ad,Me}ArO)$_3$N)(py-NO)U} (μ-O)$_2${((^{Ad,Me}ArO)$_3$N)U}], obtained by treatment of [((^{Ad,Me}ArO)$_3$N)U^{III}], the single N-anchored tris-aryloxide de-rivative of **1**, with pyridine-N-oxide. However, a similar treatment of **1** does not produce dimeric **3**. Instead, oxidation of **1** with pyridine N-oxide or trimethyl-amine N-oxide yields mononuclear U^{V} complexes **4** and **5**, [((^{nP,Me} ArO)$_3$tacn)U^{V}(O)(L)] (with L = pyN-O, Me_3N-O). As men-tioned before, all previously reported pentavalent uranium complexes of the tacn lignd systems with *tert*-butyl and ada-mantyl substituents in *ortho* position, namely [(($^{R,R'}$ArO)$_3$tacn)U^{V}(L)$_{ax}$] (with R = R_{ortho} = *t*-Bu, Ad; R' = R_{para} = *t*-Bu, Me; L_{ax} = O, NTMS, NMes) are seven-coordinate with the strongly π-donating oxo and imido ligands located on the three-fold axis of these C_3 symmetric complexes.[14] Only upon oxidation to the hexavalent state, do oxo and imido U^{VI} complexes of this ligand system display the *inverse trans influence* (ITI).[2j, 15] Consequently, their molecular structures show approximate C_s symmetry with the strongly π-donating ligand in the equatorial plane *trans* to a mutually enforced, strongly bound aryloxide ligand of the hexadentate chelate. In stark contrast, all monomeric, pentavalent uranium complexes of the new neopentyl-derivatized tacn system,

[((^{nP,Me}ArO)$_3$tacn)U^{V}(L)], have the terminal oxo and imido ligands in the equatorial plane along with the three aryloxide pendent arms of the hexadentate chelate. In the presence of the neutral, donor ligands, pyridine N-oxide, trimethylamine N-oxide, or pyridine, the coordination sphere of these complexes is completed by a usually weakly bound donor ligand in the axial position *trans* to the tacn anchor. Regardless of these drastically different coordination environments, the U–O bond distances are almost the same with 1.856(2) and 1.850(2) Å for the two independent molecules in the structure of **4**, and 1.860(2) Å for **5**, in comparison to 1.848(4) and 1.848(8) Å for [(($^{R,R'}$ArO)$_3$tacn)U^{V}(O)] (with R = Ad, *t*-Bu; R' = *t*-Bu), respectively, and other U^{V} terminal oxo complexes.[2d-f, 13] Attempts to oxidize the dinuclear complexes **3**, **6**, and **7** to obtain the corresponding complexes with [U^{V}(μ-O)$_2$ U^{VI}] or [U^{VI}(μ-O)$_2$U^{VI}] core structures only lead to isolation of mononuclear U^{VI} complexes with terminal oxo ligands, [((^{nP,Me}ArO)$_3$tacn)U^{VI}(O)$_{eq}$(L)] (with L = CF_3SO_3, **8**) and [((^{nP,Me}ArO)$_3$tacn)U^{VI}(O)$_{eq}$][A] (with A = SbF_6, **9**). U^{VI} complexes with a single terminal oxo ligand represent a rare class of complexes with few reported examples.[2h-m] The monomeric U^{VI} terminal oxo complexes **8** and **9** possess similar coordination environments to **4** and **5** as well as to known complexes of the *tert*-butyl and adamantyl-derivatized tacn systems (with complex **9** missing the axial ligand).[2j] As in **4** and **5**, the terminal oxo ligand in **8** is in the equatorial position along with the three aryloxides, and the weakly coordinating triflate counter ion is bound in axial position *trans* to the tacn anchor. The very short bond U–O$_{oxo}$ (1.794(2) in **8** *vs.* 1.811(2) Å for [(($^{t\text{-Bu},t\text{-Bu}}$ArO)$_3$tacn)U^{VI}(O)($CF_3COO$)] and 1.836(6) Å for [(($^{t\text{-Bu},t\text{-Bu}}$ArO)$_3$tacn)U^{VI}(O)][$SbF_6$]) is due

Table 1. Selected bond distances and angles for the mononuclear complexes 1, 2, 4, 5, 8, and 9.

complex	**1** (Å/°)	**2** (Å/°)	**4**[(1)] (Å/°)		**5** (Å/°)	**8** (Å/°)	**9**[(1)] (Å/°)	
U–O$_{oxo}$	–	–	1.856(2)	1.859(2)	1.860(2)	1.794(2)	1.791(6)	1.800(6)
U–O$_{phenol,av}$	2.287	2.215	2.186	2.198	2.204	2.101	2.088	2.101
U–O$_{ligand}$	2.669(2)	–	2.412(2)	2.407(2)	2.360(2)	2.436(2)	–	–
U–N$_{imido}$	–	1.979(3)	–	–	–	–	–	–
U–N$_{tacn,av}$	2.517	2.789	2.856	2.861	2.867	2.747	2.613	2.625
U–N$_{ligand}$	–	2.583(4)	–	–	–	–	–	–
U$_{oop}$	–0.362	–0.408	–0.420	–0.351	–0.200	–0.388	–0.758	–0.709
O/N$_{oop}$	–	+0.285	–0.209	–0.063	+0.240	–0.266	–0.504	–0.339
O/N–U–O$_{trans}$	–	148.80(12)	161.29(8)	160.46(8)	160.87(10)	160.73(8)	149.7(3)	147.8(3)
O$_{cis}$–U–O$_{cis}$[(2)]	–	157.00(10)	157.92(7)	161.86(7)	161.26(8)	158.04(7)	137.9(2)	140.9(2)

(1) Two independent molecules in the unit cell of **4** and **9**.
(2) O$_{cis}$ is the aryloxo arm *cis* to the terminal oxo/imido ligand

Table 2. Selected bond distances and angles for the dinuclear complexes 3, 6, and 7.

complex	**3** (Å/°)	**6** (Å/°)	**7** (Å/°)
U(1;2)–O_{oxo}	2.0354(12), 2.1815(11)	2.1259(17), 2.1928(16); 2.2012(16), 2.1445(16)	2.115(3), 2.169(3); 2.179(3), 2.115(3)
U(1;2)–$O_{phenol,av}$	2.1827	2.3822; 2.3582	2.247; 2.258
U(1;2)–$N_{tacn,av}$	2.8017	2.805; 2.784	2.811; 2.811
U(1)–U(2)	3.4222(3)	3.5090(4)	3.4653(5)
$U(1;2)_{oop}$	−0.219	−0.224; −0.181	−0.179; −0.138
O/N_{oop}	+0.263	+0.610; +0.636	+0.365; +0.470
$\pi-\pi$ / $\pi-C_{nP,tacn,av}$ [(1)]	3.623 (π-π)	3.730 (π-$C_{nP,tacn}$)	3.758, 3.655 (π-π)
U(1;2)–O–U(2;1)	108.45(5)	108.36(7); 107.99(7)	108.00(13); 107.60(12)
O–U(1;2)–O	71.55(5)	72.05(6); 71.54(6)	72.30(11); 72.09(11)
∢U–$(O)_2$–U [(2)]	0.00	2.23	0.90
O/N–U(1;2)–O_{trans}	159.97(5)	148.65(6); 149.54(6)	159.87(11); 157.94(11)
O_{cis}–U(1;2)–O_{cis} [(3)]	158.38(4)	156.55(6); 152.16(6)	158.77(12); 158.39(11)

[(1)] Distance of the aromatic ring to the carbon atom from the neopentyl-group or the tacn ring, where a π-CH bond interaction is possible.
[(2)] Torsion angle
[(3)] O_{cis} is the aryloxo arm *cis* to the terminal oxo/imido ligand

to the ITI and results from the mutually reinforced bonding within the near linear O_{ArO}–U–O_{oxo} arrangement (160.73(8)° in **8** *vs.* 159.67(6)° for [(($^{t\text{-Bu},t\text{-Bu}}$ArO)$_3$ tacn)U^{VI}(O)(CF_3COO)] and ~149° for [(($^{t\text{-Bu},t\text{-Bu}}$ArO)$_3$tacn) U^{VI}(O)][SbF_6]). Similar short U–O_{oxo} bond distances have been reported in other U^{VI} terminal oxo complexes.[2i, 2l] For complex **9**, the SbF_6 counter anion is not coordinated to the axial position; thus, leaving an open co-ordination site. Although the O_{ArO}–U–O_{oxo} angle in **9** is more acute at 149.7(3) and 147.8(3) °, due to the missing axial ligand, **9** still shows similarly short U–O_{oxo} bonds (1.791(6) and 1.800(6) Å). The U=NMes bond length of 1.979(3) Å in **2** is similar to those previously reported for U^V imido complexes (1.935 to 2.122 Å).[13-14] The uranium pyridine bond with 2.583(4) Å is in the range of other reported U–N bonds with neutral N-bound ligands.

The average uranium aryloxide bond lengths in complexes **2** – **9**, d(U–O_{ArO}), change with the oxidation state of the uranium ion: U^{VI} complexes **8** and **9** exhibit the shortest distances with ~2.100(2) Å, which is in the same range as found for other U^{VI} terminal oxo complexes.[2j] For U^V complexes **3**, **4**, and **5**, the bond distances are in the range of ~2.183 to ~2.215 Å, typical for U–O_{ArO} bonds in complexes of U^V.[2d, 13] In case of dinuclear **7** and **6**, the bonds elongate with the degree of reduction from ~2.225(3) Å in **7** ($U^{V/IV}$) to ~2.370(2) Å in **6** ($U^{IV/IV}$), respectively. A similar trend for the average U–N_{tacn} bond distances cannot be observed; the U–N_{tacn} bond lengths vary from ~2.747 to ~2.867 Å for all complexes; and thus, are slightly longer than those found in other uranium complexes of the tacn chelate, which are in the range of 2.67 to 2.76 Å.[10, 13, 16] Noteworthy, all new high-valent complexes, including the imido species **2** and oxo complexes **3** – **9**, feature the ITI. Here, the strongly π-donating terminal imido and oxo ligand is in plane with the three aryloxide ligands. Within this plane, the uranium aryloxide bond *trans* to the terminal oxo/imido ligand is slightly shorter (~0.06 Å) than the two other *cis* U–O_{Ar} bonds. The ITI is observed in the di-nuclear as well as in the mononuclear complexes to the same extent. In addition to the ITI, the inverse is also ob-served: the longest M–L distances are coordinated *trans* to each other (the longest M–L distance is *trans* to tacn anchor).

Electrochemical data from cyclic, linear sweep, and square-wave voltammetry were collected for all uranium complexes in THF or acetonitrile solutions, with ~ 0.1 M [N(n-Bu)$_4$][PF_6] as electrolyte and the ferrocenium/ ferrocene couple as internal standard. In addition, both the free (^{nP,Me}ArOH)$_3$tacn ligand and 2.2.2-cryptand were investigated to demonstrate their redox-inactivity. A summary of experimentally determined half-step potentials is given in the ESI. In contrast to [(($^{R,R'}$ArO)$_3$tacn)U^V(NTMS)] (with R = *t*-Bu, Ad, diamantanyl, R' = *t*-Bu, Me), the neopentyl derivative, U^V imido complex **2**, shows no redox chemistry in the accessible electrochemical window. This might be due to the different geometries (C_3 *vs.* C_s) found in the *tert*-butyl and adamantyl complexes *vs.* the neopentyl system studied here. The dinuclear bis-μ-oxo bridged **3**, however, shows a remarkable rich and unique electrochemistry, featuring two reversible redox events at half-wave potentials of $E_{½}$ = −0.08 V and −1.53 V *vs.* the Fc/Fc^+ couple (see Figure 4). The more cathodic redox wave can be unambiguously assigned to the one-electron reduction of the U^V/U^V species to the mixed-valent U^V/U^{IV} complex.

This couple also appears in the cyclovoltammogram of **7** ($E_{½}$ = −1.55 V, see ESI), and similar reduction potentials for U^V/U^{IV} complexes are known (−1.25 to −1.81 V *vs.* Fc/Fc^+).[17] The second redox wave at $E_{½}$ = −0.08 V is assigned to a one-electron oxidation to a U^V/U^{VI} complex, which is further confirmed by linear sweep. While the electrochemical reduction can be proved by a chemical reduction on a preparative scale, leading to isolable **7**, the chemical oxidation of **3** to yield the hypothetical mixed-valent $[U^V(\mu\text{-}O)_2U^{VI}]$ species has not yet been accomplished. Attempts to oxidize **3** with a large variety of oxidants and different stoichiometries only lead to monomeric U^{VI} oxo complexes (vide supra). The large separation between the U^V/U^{IV}, U^V/U^V, and U^V/U^{VI} redox couples allows the equilibrium constant for the comproportionation to the U^V/U^V complex to be estimated. With $\Delta E_{½} = |1.45\ V|$, K_c is approximately 3.25×10^{24}, suggesting strong electronic communication between the uranium centers.[18] It is likely that the highly covalent U–O bonds in the bis-μ-oxo diamond core support this electronic coupling although short M···M distances (and their resulting M–M bonds) have also been implicated in remarkably strong interactions between two transition metal centers. The large value for K_c may further explain the unusual stability of **3**, which is air-stable. Similar K_c values have been reported by Cummins *et al.* for the dinuclear nitrido-bridged U^V/U^{IV} complex ($K_c \approx 5.6 \times 10^{17}$), for which a wave separation of $\Delta E_{½}$ = ~1.05 V between the U^{IV}/U^{IV}, U^{IV}/U^V, and U^V/U^V redox couple has been reported.[18b]

Interestingly, while treatment of **3** with excess KC_8 yields the doubly-reduced, U^{IV}/U^{IV} complex **6**, the second reduction, the U^{IV}/U^V to U^{IV}/U^{IV} redox couple, is not observed in the CV of **3**. Also, isolated complex **6** is electrochemically inert, showing neither reversible nor irreversible redox events in its CV. Considering that in **6**, two potassium cations are bound to one of the bridging oxo ligands and form multiple bonding interactions with the aryloxide pendent arms of each U^{IV} moiety, it is reasonable to assume that the chemically introduced potassium ions play a major role in the stabilization of **6**, which may explain the different electrochemical and chemical behavior. While mononuclear U^{VI} oxo complexes **8** and **9** show no reversible redox chemistry in the accessible electrochemical window, complexes **4** and **5** show one reversible redox event centered at $E_{½}$ = – 0.18 and – 0.27 V, respectively, consistent with reported redox potentials for the metal-centered U^V/U^{VI} redox-couple (−0.11 to −0.19 V *vs.* Fc/Fc^+).[2j, 17] However, chemical oxidation of complex **4** with AgOTf resulted in ligand degradation and formation of a U^{VI} uranyl complex coordinated by two triflate and three pyridine-N-oxide ligands (see ESI).

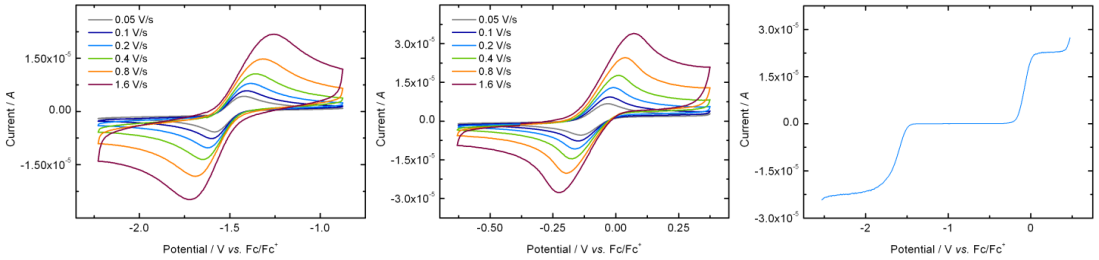

Figure 4. Reversible reduction wave (left) and reversible oxidation wave (middle) of **3** at different scan rates. Linear sweep measurement (right) in ~0.1 M $[N(n\text{-}Bu)_4][PF_6]$ in THF at room temperature. Scan was collected at 50 mV/s and with a step potential of 2 mV.

The UV/vis/NIR electronic absorption spectra of the dark brown imido complex **2**, the yellow-orange terminal oxo complexes **4** and **5**, the dark red-brown U^V–U^V complex **3**, the orange U^V/U^{IV} complex **7**, the pale green U^{IV}/U^{IV} complex **6**, and the two black U^{VI} complexes **8** and **9** were measured in THF for different concentrations from 200 to 2500 nm at 25 °C. Figure 5A displays all collected spectra over the UV/vis spectral range and Figure 5B shows excerpts of characteristic *f*–*f* transitions in the NIR spectrum. Generally, the electronic absorption spectra of complexes **2** – **7** can be divided into two regions. The first region, between 200 and 550 nm, shows intense and broad charge-transfer bands (CT) characteristic of $\pi \rightarrow \pi^*$ and $\pi \rightarrow nb_{5f}$ (nb = non-bonding), and metal-centered $5f \rightarrow 6d$ transitions above 40.000 cm^{-1} with molar extinction coefficients of $\varepsilon \sim 20\times10^3 - 70\times 10^3$ $M^{-1}cm^{-1}$ (Figure 5A).[19] A second region between 500 and 2500 nm is dominated by metal-based *f*–*f* transitions with varying intensity and molar extinctions that vary from 10 to 600 $M^{-1}cm^{-1}$ (Figure 5B).

Black, mononuclear U^{VI} oxo complexes **8** and **9** strongly absorb over the entire spectral range from 220 to 1280 nm. In the UV region, most complexes exhibit two similar features at ~250 and 300 nm with molar extinction coefficients of ~$20\times10^3 - 30\times10^3$ $M^{-1}cm^{-1}$ per uranium. In addition, dinuclear **3** and **7** show strong absorption into the visible spectrum below 600 nm, with $\varepsilon \sim 3{,}000$ $M^{-1}cm^{-1}$ per uranium (at $\lambda \sim 483$ and 388 nm, respectively), whereas monomeric U^V complexes display only weak absorption below 450 nm. The U^{VI} complexes **8** and **9** absorb strongly below 1400 nm, but as expected, no *f*–*f* transitions are observed.

.

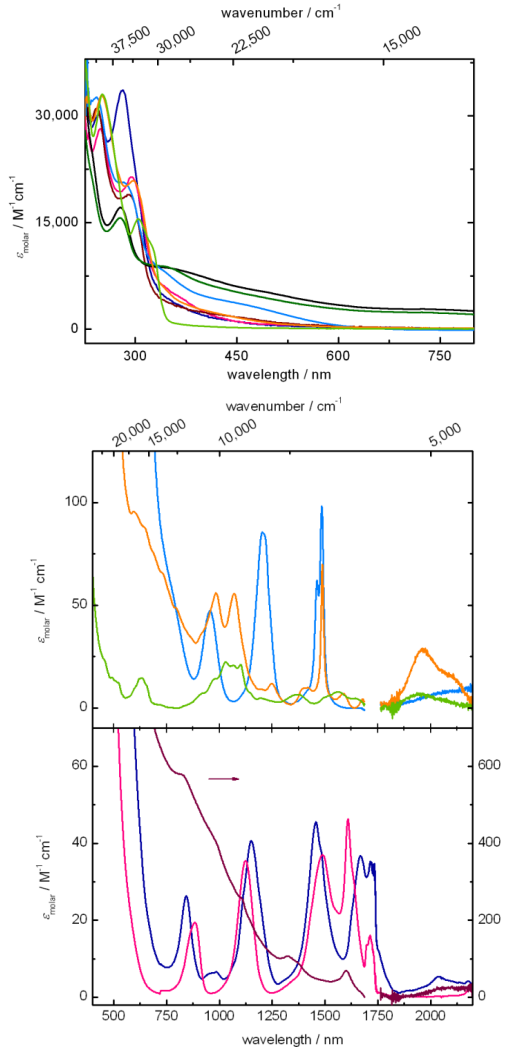

Figure 5. A) UV/vis absorption spectra of **2** (purple), **3** (blue), **4** (dark blue), **5** (pink), **6** (green), **7** (orange), **8** (black), and **9** (dark green). **B**) NIR absorption spectra. Top: **3**, **6**, and **7**. Bottom: **2**, **4**, and **5**. Extinction coefficients are reported per one uranium center.

The metal-centered *f*–*f* transitions depend on the electronic configuration of the uranium ion. U^V is simplest to understand since it possesses just one unpaired electron; hence, no electron-electron repulsion occurs. Absorptions with average molar extinction coefficients of $\varepsilon \approx 50$ $M^{-1}cm^{-1}$ per uranium, can be observed for the terminal oxo complexes **4** and **5**, as well as for the dinuclear bis-μ-oxo complexes **3** and **7**, and are

comparable to bands observed for the terminal oxo complexes [(($^{t\text{-Bu},t\text{-Bu}}$ArO)$_3$tacn)U^{V}(O)] and [(($^{Ad,t\text{-Bu}}$ ArO)$_3$tacn)U^{V}(O)].[13] Note that **7** displays both U^{IV} and U^{V} spectral features. The wider range of 840 –1670 nm for **4**, compared to 880 – 1610 nm for **5**, suggests a slightly stronger ligand field in **4**, which produces a larger splitting of the states. In stark contrast to the U^{V} oxo complexes, U^{V} imido compound **2** shows one broad absorption band, spanning from ~750 – 1700 nm, with some less-resolved superimposed features. The spectral shape and intensity ($\varepsilon \sim 70 - 580$ M^{-1}cm^{-1}) is reminiscent to the spectrum of the [(($^{t\text{-Bu},t\text{-Bu}}$ArO)$_3$tacn)U^{V}(NMes)] and [(($^{Ad,t\text{-Bu}}$ArO)$_3$tacn)U^{V}(NMes)] complexes,[13] and to other reported U^{V} imido complexes.[17, 20]

For the purposes of interpreting the NIR spectra, the U^{V} oxo complexes may be viewed as distorted octahedral complexes with the tacn anchor occupying a single coordination site as earlier noted. Of these complexes, **7** has the least distorted U$_2$(μ-O)$_2$ core with U-O distances of 2.11 and 2.17 Å; the U-O-phenoxide distances are somewhat longer at 2.25 Å. Complex 3 has a more distorted U$_2$(μ-O)$_2$ core with U-O distances of 2.07 and 2.20 Å, and **4** and **5** are strongly distorted with a short terminal oxo distances of 1.86 Å. These four complexes form a series in which the relatively symmetric bridging oxo groups in **7** begin to distort in **3** forming short U-O bond, which becomes the terminal oxo group of **4** and **5.**

The NIR spectra of pseudo-octahedral uranium complexes have previously been described[21] and the bonding has been interpreted by using a crystal field model.[22] Like **3** – **5**, dianionic [UOX$_5$]$^{2-}$ possesses a short U–O bond in a distorted octahedral coordination environment. The other related complex is the anion [U(O-*t*-Bu)$_6$]$^{-}$, which displays very similar U–OR bond lengths (2.05 Å to 2.24 Å) to that observed here.[23] Therefore, the NIR spectrum of **7** should be expected to be similar to that of [U(O-*t*-Bu)$_6$]$^{-}$, and the spectra of 3-**5** should be related to **7** in the same way that [UOX$_5$]$^{2-}$ are related to [UX$_6$]$^{-}$.

The splitting of the *f*-orbitals in a pseudo-octahedral f^1 complex can be described as shown in Figure 6, following the scheme developed by Selbin and Sherrill.[22] In contrast to the complexes described by Selbin and Sherrill, the f_{xyz} orbital participates in bonding in **3** – **5** and **7** (primarily with the tacn amine nitrogen atoms), so the A_{2u} state is antibonding in **3** – **5** and **7** rather than non-bonding. Using the labels for octahedral symmetry (Figure 6b), the NIR spectrum of **7** may be assigned by reference to the spectrum of [U(O-*t*-Bu)$_6$]$^{-}$. The sharp feature at 1487 nm is the $\Gamma_7 \rightarrow \Gamma_{7'}$ transition (6725 cm^{-1}), the absorption bands at 984 nm and 1072 nm are the two branches of the $\Gamma_7 \rightarrow \Gamma_{8'}$ transition (9745 cm^{-1}) (this peak is always split in the octahedral U^{V} complexes), and the shoulder at 795 nm is assigned to the $\Gamma_7 \rightarrow \Gamma_6$ transition (12580 cm^{-1}).

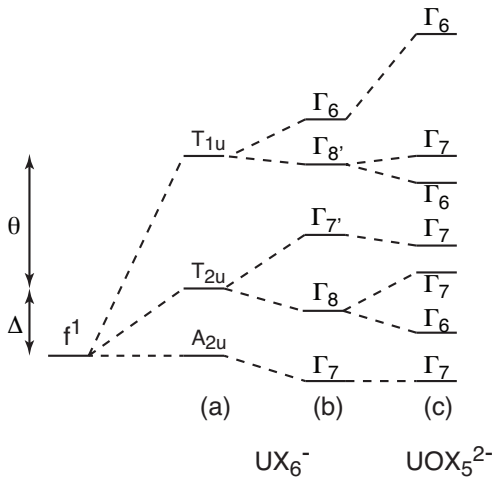

Figure 6. Splitting of an f^1 system due to (a) O_h ligand field of [UX$_6$]$^{-}$, (b) effect of spin-orbit coupling, (c) effect of replacing X with a terminal oxo ligand. Diagram after Selbin and Sherrill.[22]

Going from **7** to **3** to **4** and **5**, one bridging oxo ligand becomes the short terminal oxo ligand, which is analogous to moving from [UX$_6$]$^{-}$ to [UOX$_5$]$^{2-}$. Consequently, the Γ_6 state in **7** increases in energy in **3** forming the shoulder at 750 cm^{-1} and is unobserved in **4** and **5** (it should be ~625 nm, but is obscured by the CT bands). The Γ_8' feature around 1000 nm in **7** splits in **3**-**5** as the distortion increases forming a Γ_6 peak ~1150 nm and a Γ_7 peak ~900 nm. The energy of $\Gamma_{7'}$ is roughly in the same in all complexes ~1450 cm^{-1}. A new peak appears in **4** and **5** ~1600 cm^{-1}, which is presumably the Γ_7 peak produced by splitting the Γ_8 peak in **7**, which is in the IR.

Using the assigned energies of the $\Gamma_{7'}$, $\Gamma_{8'}$, and Γ_6 states of **7** and its average g-value (1.080), the crystal field of **7** may be modeled as previously done for [U(O-*t*-Bu)$_6$]$^{-}$ (Table S23). The fitting parameters are spin-orbit coupling, ζ, and two splitting parameters θ and Δ, illustrated in Figure 6. ζ was almost identical to that of [U(O-*t*-Bu)$_6$]$^{-}$, which implies that bonding is equally covalent in both complexes. Likewise, θ, which is essentially the destabilization of the f-orbitals due to σ-bonding, is almost identical in both complexes. On the other hand, Δ, which is the destabilization of the f-orbitals due to π-

bonding, is much smaller in **7** (2166 cm^{-1}) than in $[U(O\text{-}t\text{-}Bu)_6]^-$ (3779 cm^{-1}). This difference may be rationalized by noting that each *t*-butoxide ligand may form two π-interactions with the U center, while the phenoxide and bridging oxo ligands may only form a single π-interaction with each uranium center. Overall, the electronic structure and bonding in **7** are very similar to that of $[U(O\text{-}t\text{-}Bu)_6]^-$ with the exception that π-bonding is somewhat weaker in **7**.

Although the *f–f* transitions in **2** are significantly more intense (~10×) than for the U^V complexes **4** and **5**, the their CT transitions are equally intense, which is contrast to recent reports of Kiplinger *et al.*.[24] The comparatively high molar extinction coefficients for these U^V complexes in contrast to other U^V compounds, like pseudo-octahedral U^V halide complexes (ε = 5 – 22 $M^{-1}cm^{-1}$), may arise from the low C_s symmetry, leading to a relaxation of the electric dipole selection rules. The same behavior was observed for Kiplinger´s complexes, having ε values ranging from ~ 100 to 400 $M^{-1}cm^{-1}$.[25] Also, the nature of the uranium-ligand bond significantly affects the intensities of the absorption bands. While simple σ-donor ligands typically lead to low intensities, more covalently bound π-donor ligands, such as complexes with terminal oxo and imido ligands, possess larger extinction coefficients due to orbital-mixing and relaxation of the Laporte's rule ("intensity stealing").[26]

The most salient feature in the spectrum of **6** is the lack of the distinctive U^V transitions observed in **3-5** and **7**. This is not only immediately indicative for the complete reduction of pentavalent **3** and mixed-valent **7** to fully tetravalent **6** but is in good agreement with the structural observation of a symmetric $[U^{IV}(\mu\text{-}O)_2U^{IV}]$ core with relatively long but equal U–O bond distances, indicating weaker U–O bonds with little to no double-bond character. Instead, the spectrum of **6** is reminiscent of "standard" U^{IV} complexes of the tacn and single N-anchored tris(aryloxide) complexes, featuring a large number of low-intensity *f–f* transitions over the entire spectral range. The U^{IV} ion with its $5f^2$ electronic configuration experiences electrostatic repulsion of the two *f*-electrons as well as significant spin-orbit coupling, which leads to a large number of levels within $^3H_4$ the ground state. In addition, and depending on symmetry and crystal-field strength, the levels are further split into (2J + 1) states. In U^{IV}, the crystal-field splitting is typically between 100 and 2000 cm^{-1},[19] which is in the same order of magnitude as the spin-orbit coupling energy. This leads to a significant mixing of states; consequently, a large number of *f–f* transitions in the visible to NIR region. Accordingly, **6** possesses several unresolved bands from 450 to 1950 nm with low molar extinction coefficients of $\varepsilon \approx 10 - 50$ $M^{-1}cm^{-1}$.[27]

The nature of the $U–O_{oxo}$ bonds in complexes **3** – **9** was further probed by IR and Raman vibrational spectroscopy. It should be noted that employing $C^{18}O_2$ in the multiple bond metathesis reaction enabled the synthesis and isolation of the ^{18}O labeled bis-μ-oxo-bridged dinuclear complexes **3**, **6**, and **7** and allowed – for the first time – the unambiguous assignment of the vibrational signature of the $[U(\mu\text{-}O)_2U]$ diamond core structural motif.

The IR spectra, performed on solid samples (KBr pellet, see ESI), are all dominated by the spectrum of the relatively complex hexadentate chelating ligand system in $[((^{nP,Me}ArO)_3tacn)U(L)]$. Consequently, all complexes show very similar vibrational spectra, except for a single absorption band in the fingerprint region at 748 cm^{-1} for **4** and 741 cm^{-1} for **5**, respectively (see ESI). This feature cannot be observed in complexes **2**, **3**, **6** – **9**, and is therefore assigned to the terminal oxo–uranium stretching vibration, ν(U=O). Although labeling studies were not performed on **4** and **5** (these complexes were not synthesized with $C^{18}O_2$), the energy of the assigned ν(U=O) peak is in good agreement with literature reports for this absorption band.[2c, 2h] Unambiguous identification of the metal-oxygen bond stretching frequencies in the $[U(\mu\text{-}O)_2U]$ diamond core of dinuclear complexes **3**, **6**, and **7**, as well as the U=O group in their mononuclear oxidation products **8** and **9**, was achieved through the use of isotopic labeling with $C^{18}O_2$ (95 % enriched in 18-O). Thus, comparison of the parent complexes with their 18-O labeled isotopomers (18-O isotopomer denoted with *) **3***, **6***, **7***, **8***, and **9*** (see ESI) revealed two strong isotope-sensitive bands between 500 and 648 cm^{-1} (see ESI). These vibrational bands were assigned to the symmetric stretching and symmetric deformation vibrations. Similar values between 600 and 900 cm^{-1} are reported for transition metal complexes containing the $[M(\mu\text{-}O)_2M]$ diamond core moieties (M = Mn, Co, Os).[28] For the mononuclear U^{VI} oxo complexes **8** and **9**, a shift of one vibrational band from 829 to 818 cm^{-1} and 826 to 822 cm^{-1} for

the isotopomers **8*** and **9*** was observed. These values are comparable to those reported for the terminal U^{VI} oxo complexes [$((Me_3Si)_2N)_3U^{VI}O(X)$] (with X = F, Cl, Br) re-ported by Schelter *et al.* ($\nu_{U=O}$ = 859 – 882 cm^{-1}).[2m] The results obtained from IR vibrational spectroscopy agree well with the ones obtained from X-ray crystallographic studies and verify that the overall U=O bond order is lowered from the terminal oxo U^{VI} (1.794 (2), 1.791(6) and 1.800(6) Å) to the terminal oxo U^{V} (1.8561(18), 1.8586(18) and 1.860(2) Å) to the dinuclear bis-μ-oxo bridged complexes.

Raman spectroscopy measurements for all labeled and unlabeled complexes were conducted in solid state at room temperature. Due to strong emissions for all complexes except for **3** and its 18-O isotopomer **3***, no meaningful Raman spectra could be obtained. For **3** and **3***, however, a set of features are evident in the spectra, but only one shift is sensitive to 18-O substitution moving from 622 cm^{-1} to 584 cm^{-1} (588 cm^{-1} calculated for a simple U–O harmonic oscillator) and is assigned to the "breathing mode" of the diamond core moiety (see ESI). Similar values and assignments can be found in the literature for [M(μ-$O)_2$M] diamond cores in transition metal complexes. For example, Tolman *et al.* synthesized [Cu (μ-$O)_2$Cu] complexes with Raman shifts from 604 – 647 cm^{-1} for the unlabeled and 570 – 624 cm^{-1} for the 18-O labeled complex.[29] Further complexes show similar shifts for the unlabeled (700 – 590 cm^{-1}) and 18-O labeled (634 – 560 cm^{-1}) [M(μ-$O)_2$M] diamond core moiety with M = Fe, Mn, Ni.[30]

Until recently, the magnetism of U^{V} compounds has not been extensively investigated due to the difficulty in pre-paring complexes in this oxidation state. This has been particularly true for coordination complexes of low symmetry and for magnetically coupled systems.[6e] More recently, the development of novel synthetic routes to stable U^{V} complexes has lead to an expansion in the studies of the magnetism of this oxidation state.[2f, 5a, 5c, 6f, 31] Nevertheless, exchange coupled systems remain rare.[6] Thus, the complexes described in this paper offer a unique opportunity to study the magnetic properties of this novel series of dinuclear uranium coordination complexes with similar uranium coordination environments. Reproducible temperature-dependent and field-dependent magnetization data were collected for several isolated and independently synthesized samples. Even in analytically pure samples, all complexes exhibit small amounts of an unidentified paramagnetic impurity. These ubiquitous impurities may occur from minute uncoupled impurities (for the dinuclear complexes), ferrites, especially magnetite, from stainless steel lab equipment, and/or defects at the surface of the micro-crystallites.[32] The presence of impurities is mainly noticeable in the low temperature magnetic susceptibility of **3** and **6** since both of these complexes have very small magnetic moments at low temperature.

The magnetic susceptibilities of these complexes are best understood using the van Vleck equation (eq 1), where χ_{mol} is the magnetic susceptibility of the complex, χ_o is the magnetic susceptibility of a thermally occupied state at energy E_J, the α term is the temperature independent paramagnetism (TIP) due to low lying excited states, and the other symbols have their usual meanings.[33] The magnetic susceptibility of a given complex is just the Boltzmann distribution of the susceptibilities of the occupied states, and the susceptibility of each state has a temperature dependent term proportional to g^2 and a temperature independent term that is inversely proportional to the energies of the excited states. In uranium complexes, some excited states are typically at low energy and become thermally populated below 300 K. In addition, the TIP term α is often large in these systems due to the low energies of the excited states.

$$\chi = \frac{\sum_j \chi_j e^{-\frac{E_j}{kT}}}{\sum_j e^{-\frac{E_j}{kT}}}, \text{ where } \chi_j = N\left(\frac{\mu_B^2 g^2 S(S+1)}{3kT} - \alpha\right) \text{ with}$$

$$\alpha = \sum_{j\neq k} \frac{2\left|\langle\phi_k|\boldsymbol{L}+2\boldsymbol{S}|\phi_j\rangle\right|^2}{E_j - E_k} \qquad \text{(eq 1)}$$

When the magnetic susceptibility is plotted as χT *vs.* T, the occupancy of the low-lying states is often discernable by the change in slope of χT *vs.* T. At low temperatures, where only a single state is occupied, χT will be linear in T. The TIP term can be determined from the slope, and the average value of g may be determined by extrapolating χT to zero K (χT at 0 K). As the temperature increases and low-lying states become thermally populated, the slope of χT *vs.* T decreases (the TIP terms of the ground and excited states cancel), and the slope of χT *vs.* T changes (the plot curves) until the occupied states are again in thermal equilibrium, at which point χT *vs.* T is again linear. If the total splitting of the *f*-orbitals by the crystal field is significantly smaller than kT at room temperature, all of the states in the ground multiplet (e.g. $^2F_{5/2}$ for U^{V}) are in thermal

equilibrium, and the magnetic moment may be compared to that of the free ion. Covalent interactions decrease the magnetic moment by reducing the orbital angular momentum of the complex, which decreases both g and α in eq 1.[34]

The strength of the crystal field has a large effect of the magnetic susceptibility of the complex. If the ligands create a crystal field that is large compared to kT at 300 K, only the lowest lying *f*-states will be occupied, and the magnetic susceptibility will be significantly different from that of the free-ion. A plot of χT *vs.* T will be significantly temperature dependent at 300 K, if this is the case, due to TIP created by slightly higher lying excited states. A strong crystal field will also result in mixing of the lowest lying free-ion states (e.g. $^2F_{5/2}$ and $^2F_{7/2}$ for U^V), resulting in a further deviation of the magnetic moment from that of the free ion.

Magnetic moments at room temperature and extrapolated to zero K are given in the ESI for . The magnetic susceptibilities of complexes **4** and **5** are typical of U^V complexes stabilized by oxo ligands (see ESI).[2e, f, 13] In all of the complexes, the magnetic moment at 300 K is significantly reduced from the free ion moment of 2.54 μ_B for $^2F_{5/2}$. Also, χT has substantial temperature dependence at 300 K, which is consistent with the large crystal field splitting observed in the NIR. In **4**, χT is linear in T from 0 to 20 K, at which point the slope changes until χT is again linear in T from 150 K to 300 K, which indicates that the first excited state is ~50 K (35 cm^{-1}) above the ground state and that no other low-lying excited states become populated below 300 K. In **5**, on the other hand, χT is linear in T from 5 to 300 K with a slight deviation below 5 K. In this case, the first excited state is either very low in energy and is in thermal equilibrium with the ground state at 5 K, or the first excited state does not become significantly populated below room temperature. Given the relatively large splitting of the *f*-orbitals observed in the NIR (>5000 cm^{-1}) relative to kT at 300 K (209 cm^{-1}), the latter explanation seems more likely.

The ground states of these complexes have similar magnetic moments to those of octahedral $[UX_6]^-$ complexes, which vary from 0.63 μ_B for $[U(OR)_6]^-$ to 1.24 μ_B for $[UR_6]^-$ as determined from the g-values of their ground states.[5a] This similarity supports the analogy with octahedral f^1 ions presented when discussing the electronic spectra and suggests that the half-occupied orbital is largely f_{xyz} in character. The lack of low-lying states in **5** is also consistent with the picture.

The three dinuclear complexes (**3**, **6**, and **7**) show remarkably different magnetic behavior, clearly observable in the plot χT *vs.* T (see Figure 7). The χ *vs.* T plot of complex **3** exhibits the magnetic behavior of an anti-ferromagnetically coupled dinuclear complex with a Néel temperature (T_N) of approximately 70 K. The (reproducible) upturn in susceptibility below 20 K is attributed to the presence of paramagnetic impurities. At room temperature, **3** has a magnetic moment per U that is comparable to the other U^V complexes.[2e, f, 13] Interestingly, the χT *vs.* T plot of **3** is linear from 100 K to 300 K, which suggests that no further states become thermally populated over this range. The strong temperature dependence of χT of **3** at 300 K suggests that only the lowest crystal field states of each ion – possibly only a single crystal field state – are populated below room temperature, which is consistent with the NIR spectrum of this ion. Magnetic exchange in this complex will be addressed below.

The magnetic susceptibility of the doubly-reduced complex **6**, $[U^{IV}(\mu\text{-}O)_2U^{IV}]$, shows no evidence of exchange coupling. Instead, **6** displays characteristic behavior for isolated tetravalent U^{IV} complexes.[2g, 35] Specifically, χT of **6** is linear to 70 K with χT at zero K approximately equal to zero, which implies that the g-value of the ground state is zero. In addition, the χ *vs.* T plot of **6** displays a plateau below 70 K, which is masked by the presence of paramagnetic impurities (*vide supra*). The free-ion ground state for U^{IV} is $^3H_4$, which is split by the ligand field into three non-Kramers doublet states and one singlet state. The singlet state has a g value of zero and displays only TIP, which is consistent with the ground state magnetic susceptibility observed for **3**. In octahedral crystal fields, U^{IV} displays a singlet ground state,[36] which further supports the postulate that these complexes may be viewed as distorted octahedra, at least from the perspective of their electronic structures. A singlet ground state in **6** is consistent with the observed lack of coupling in this molecule since singlet states have no net spin and thus do not display exchange coupling. To estimate the energy gap between the ground and excited state, it is assumed that an excited state population of less than 5 % leads to no change in magnetic susceptibility.[37] Applying the Boltzmann distribution, a state energy gap of ~125 cm^{-1} can be expected.[37-38] As with the other complexes, χT of **6** is

strongly temperature dependent at 300 K, which is consistent with the large crystal field splitting observed in its NIR spectrum.

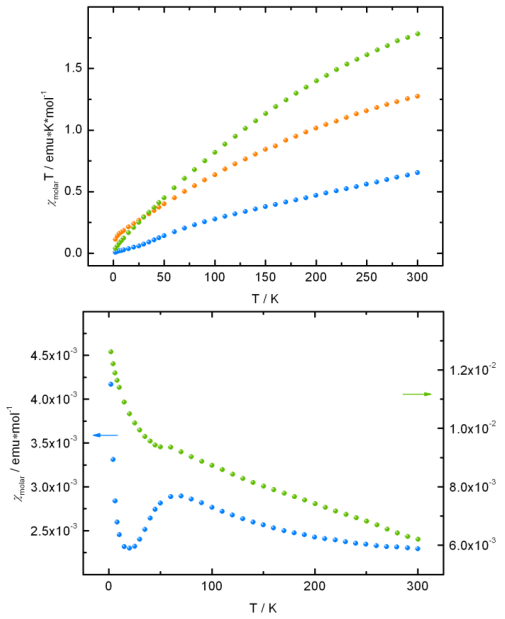

Figure 7. Temperature-dependent magnetic susceptibility data for **3** (blue), **6** (green), and **7** (orange) shown as χT *vs.* T (left) and χ *vs.* T (right). For the χ *vs.* T plot, the scale for **3** is on the left and the scale for **6** is on the right.

The mixed-valent U^{IV}/U^{V} complex **7** shows magnetic behavior reminiscent of both U^{IV} and U^{V}, which is in perfect agreement to its electronic absorption spectrum (*vide supra*). The product χT of **7** is linear in T from 6 to 100 K with a small deviation below this value. Therefore, only a single state is (or two almost degenerate states are) thermally occupied over this range, which is consistent with both the behavior of **6** and with the monomeric U^{V} species **5**. At 300 K, as one might expect, the magnetic moment is intermediate between those of the U^{IV} complex **6** and of the monomeric U^{V} complexes. For **7**, χT does not become linear at higher temperature, most likely due to the changing thermal populations of the low-lying states, which is similar to the behavior of **6**. As with the other complexes, χT is strongly temperature dependent at 300 K, which suggests that only the lowest lying states are thermally occupied and is consistent with the large splitting of the *f*-states observed in the NIR.

The Néel temperature T_N of **3** is considerably larger than typically observed for U^{V} complexes.[6a, 6e, f, 39] Only T_N of the U^{III} inverse sandwich complex described by Cummins *et al.* is larger at 110 K. Ideally, one would like to quantify the exchange coupling in this system; however, this goal is complicated by several factors. The contribution of the paramagnetic impurity must be accounted for, which is straightforward. Exchange coupling may be quantified in centrosymmetric systems, such as **3**, if the magnetic anisotropy and magnetic susceptibility of an isolated magnetic ion (diamagnetic substitute) is available.[40] In the case of **3**, the ideal diamagnetic substitute would be the analogous complex with one of the uranium atoms replaced by protactinium,[41] which is prohibitively difficult. The role of the diamagnetic substitute is to account for the effect of the crystal field on the magnetic susceptibility of the ions in the coupled pair. Therefore, a complex with a similar structure to **3** but without a neighboring magnetic ion would be useful. While **4** and **5** are similar to **3**, the uranium terminal oxo distances in the mononuclear systems are considerably shorter than the short U–O bond in **3**. On the other hand, the structure of **7** is quite similar to that of **3** and could be a useful diamagnetic substitute if one can account for the susceptibility of the U^{IV} center. Since the U^{IV} centers in **6** are not exchange coupled (at least their singlet ground states are not coupled), it is possible that this complex can be used to correct for the presence of the U^{IV} center in **7** by simply subtracting half of the susceptibility of **6** from that of **7**. This approach will fail if the U^{V} and U^{IV} centers in **7** are exchange coupled, which is unlikely given the singlet ground state of U^{IV} in **6**. As shown in Figure 8, this procedure does result in the typical magnetic susceptibility of a U^{V} ion. χT is linear over the entire temperature range, which is consistent with occupancy of only a single crystal field state below 300 K; as seen with mononuclear **5**.

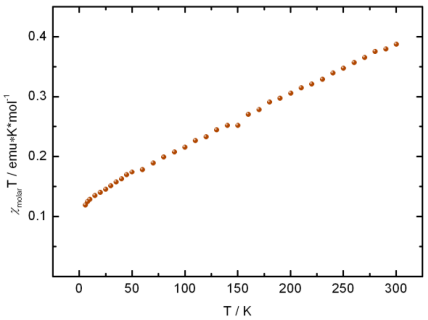

Figure 8. Magnetic susceptibility of **7** minus half of the magnetic susceptibility of **6**..

In addition to the magnetic susceptibility of the diagmangetic substitute, its magnetic anisotropy is needed and may be obtained from the EPR spectrum. As shown in Figure 9, **7** displays the rhombic EPR spectrum of a low symmetry complex,

and its anisotropy, γ, is given by g_{min}/g_{max} = 0.39. The magnetic moment of the ground state may be determined from the EPR spectrum using $4\mu_{eff}^2 = (g_1^2+g_2^2+g_3^2)$. The resulting value, μ_{eff} = 1.01 μ_B, may be compared with μ_{eff} (0 K) determined from a linear fit of the data shown in Figure 8 (1.00 μ_B). The agreement between these values supports the notion that the magnetic susceptibility of the U(V) center in **7** may be modeled by subtracting half the susceptibility of **6** from that of **7**.

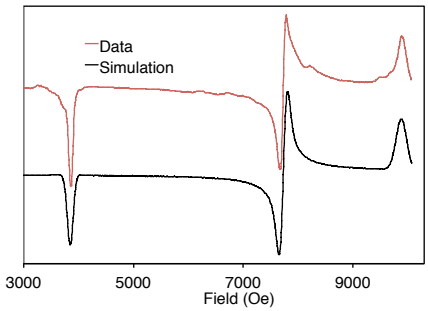

Figure 9. X-band EPR spectrum of **7** and simulation. (g_1 = 1.712, g_2 = 0.851, g_3 = 0.666).

In **3**, with strong, antiferromagnetic exchange, the standard Heisenberg-Dirac-van Vleck (HDVV) spin Hamiltonian can be applied to the spins, $\mathcal{H} = -2\mathcal{J}\,\mathbf{S_1}\bullet\mathbf{S_2}$, where $2\mathcal{J}$ is the difference in energy between the singlet and triplet states, and **S** is the spin of the electron. In molecules such as **3** with unquenched orbital angular momentum, **L**, and strong spin-orbit coupling, the total angular momentum, **J**, rather than **S** is applicable, and the system is described using an effective spin, $\hat{\mathbf{S}}$, which accounts for the degeneracy of the state and is related to the angular momentum by the g-values and Landé factor.[42] Since the states of the individual U centers in **3** are Kramers doublets, $\hat{\mathbf{S}}$ = 1/2, the resulting effective spin Hamiltonian is anisotropic, $\hat{H} = 4\hat{J}_\perp\hat{S}_{\perp1}\hat{S}_{\perp2} + 2\hat{J}_\parallel\hat{S}_{\parallel1}\hat{S}_{\parallel2}$, where $\hat{J}_\parallel = (g_\parallel/g_J)^2(g_J\text{-}1)^2\mathcal{J}$ and $\hat{J}_\perp = (g_\perp g_J)^2(g_J\text{-}1)^2\mathcal{J}$, which leads to $\hat{J}_\perp = (g_\perp/g_\parallel)^2\,\hat{J}_\parallel$. In other words, the magnetic anisotropy of the isolated ion produces highly anisotropic coupling of the effective spins. In contrast to the anisotropy, the paramagnetic impurity is easy to account for. In this case, the magnetic susceptibility of the three lowest data points was fit to the Curie-Weiss equation, $\chi = C/(T-\theta)$, to determine θ, which was held constant. The value of C was allowed to vary in the fit to account for the paramagnetic impurity. In addition to the Curie constant of the impurity, the parameters used in the fit are $\mathcal{J}$ (the HDVV coupling constant) and w (a weighting factor applied to the susceptibility of the diamagnetic substitute to account for weighing errors). The fit of the susceptibility of **3** using this approach is shown in Figure 10. The value of $2\mathcal{J}$ determined for **3** has no physical significance in and of itself because the large crystal field in this complex mixes the $^2F_{5/2}$ and $^2F_{7/2}$ states, so g_J is not that of either state. The values of $\hat{J}_\parallel$ and $\hat{J}_\perp$ are still meaningful -- $2\hat{J}_\parallel$ is the singlet-triplet gap when the magnetic field is parallel with the axis with g=1.71, and $2\hat{J}_\perp$ is the gap when the magnetic field is perpendicular. The small value of $\hat{J}_\perp$ results in an increase in the magnetic susceptibility of **3** at low temperature (~15 K); however, the increase is relatively small because $\chi_\perp$ is small ($\chi_\perp \propto g_\perp^2$). The main effect is that χ decreases to zero less rapidly below T_N than it would if $\hat{J}_\perp = 0$ (Ising coupling) or if $\hat{J}_\perp = \hat{J}_\parallel$ (Heisenberg coupling).

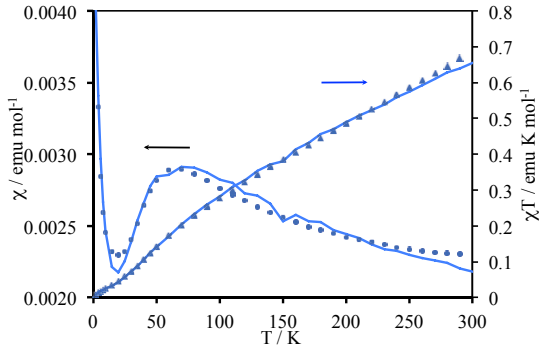

Figure 10. Fitting of the temperature-dependent SQUID magnetization data of **3** with γ = 0.39 (from EPR), C = 0.044, w = 0.92, and $\hat{J}_\parallel = -67$ cm^{-1} ($\hat{J}_\perp = \gamma^2\hat{J}_\parallel = -10$ cm^{-1}).

The T_N of 70 K in **3** is the second highest reported for a uranium compound; only the 110 K T_N observed in the arene-bridged U^{III} dimer reported by Cummins *et al.* is greater.[6i, 9] Only few solid-state materials, such as UCl_3 and UBr_3, with ordering temperatures of 22 and 15 K, respectively, have been studied.[43] Few coordination complexes of U^V are known that show f^1–f^1 coupling between the uranium centers *via* the bridging ligand. In 1989, Andersen and Edelstein *et al.* presented the first U^V complex, [{$(MeC_5H_4)_3U$}$_2$-(μ-1,4-$N_2C_6H_4$)], showing antiferromagnetic coupling. In this case, the U^V centers are bridged by 1,4-di-imidobenzene, which yields to a T_N of ~20 K.[6e] In 2008, Mazzanti *et al.* reported the dimeric U^V uranyl complex, $[UO_2(dbm)_2K(18C6)]_2$, in which two uranyl–oxos acting as bridging ligands.[6c] Herein, the T_N is ~5 K, suggesting relatively weak antiferromagnetic exchange coupling; stronger coupling was observed in a structurally

related trimeric complex with a T_N of 10 K.[39] Only recently, in 2012, Love, Arnold and co-workers studied the dinuclear complex $[(Me_3SiOUO)_2(L)]$, L = polypyrrolic macrocycle, and reported a strongly antiferromagnetic coupling, with an ordering temperature of 17 K.[6f] Ordering temperatures in a comparable temperature range to **3** (70 K) only occur in uranium solid state compounds, *cf.*, UO_2 (28.7 K), UN (53 K) or UBi (285 K).[44]

CONCLUSIONS

In 2008, we reported the synthesis of mononuclear U^V terminal oxo complexes *via* multiple-bond metathesis of a high-valent U^V imido complex with CO_2.[13] With the introduction of the neopentyl-derivatized tris(aryloxide) tacn chelate, $(^{nP,Me}ArO)_3tacn^{3-}$, (instead of ortho *tert*-butyl or adamantyl substituents),[10] the U^V imido $[((^{nP,Me}ArO)_3tacn)U^V(NMes)_{eq}(py)_{ax}]$ not only shows an entirely different and surprising coordination mode but also leads to a 'different' reaction product when exposed to an atmosphere of CO_2. Multiple-bond metathesis reaction of the imido complex with CO_2 still eliminates isocyanate but the terminal oxo complex formed *in situ* dimerizes to yield the principal dinuclear complex **3** with a diamond core $U^V(\mu\text{-}O)_2U^V$ structural motif. This reaction selectivity is likely due to the more flexible neopentyl substituents and to additional π-C–H interactions of the phenolate rings and the neopentyl groups, which stabilize the dinuclear diamond-core.[10] Complex **3** can be reduced by one or two electrons to yield the mixed-valent U^{IV}/U^V bis-μ-oxo complex, $[K(crypt)][\{((^{nP,Me}ArO)_3tacn)U^{IV/V}\}_2(\mu\text{-}O)_2]$ (**7**), and the U^{IV}/U^{IV} bis-μ-oxo complex, $K_2[\{((^{nP,Me}ArO)_3tacn)U^{IV}\}_2(\mu\text{-}O)_2]$ (**6**), respectively. Due to the convenient synthesis *via* U=NR/CO_2 multiple bond metathesis, access to the 18-O labeled iso-topomers is provided by the use of 18-O labeled $C^{18}O_2$. Thus, for the first time, the unambiguous assignment of the vibrational signature of the $[U(\mu\text{-}O)_2U]$ diamond core structural motif in **3**, **6**, and **7** has been accomplished. Invariably oxidation of the dinuclear U^V/U^V complex gave mononuclear U^{VI} oxo complexes, independent of the coordination chemistry of the oxidant anion. Oxidation of **3** lead exclusively to formation of monomeric U^{VI} oxo complexes, with the counter ion either coordinated (triflate) or not (SbF_6), depending on the oxidizing agent. Additionally, two mononuclear U^V oxo complexes were synthesized independently. The UV/vis/NIR electronic absorption spectra of the pentavalent complexes **3** – **5** can be understood by considering the tacn anchor to be a single ligand. This assumption means that the coordination sphere of these complexes can be considered distorted octahedra. In this symmetry, the half-occupied orbital is f_{xyz}, and the *f*–*f* transitions may be assigned by analogy to the simple and well-under-stood $[UX_6]^-$ and $[UOX_5]^{2-}$ systems. The energies of the low-lying *f*–*f* transitions show that the splitting of the *f*-orbitals due to their interactions with the ligands is large compared with kT at room temperature. Magnetic measurements of the paramagnetic complexes **2** – **7** are consistent with large splitting of the *f*-orbitals observed in the NIR. Specifically, only a single, occupied state is observed to relatively high temperature in most of these complexes and the values of μ_{eff} at 300 K are considerably smaller than that of the free ion. Most remarkable, in this series of bis-μ-oxo diuranium complexes, the U^V/U^V dimer, **3**, displays unusually strong antiferromagnetic coupling with T_N = 70 K. The magnetic susceptibility was fit using the magnetic susceptibility of the U^V center in **7** to model the magnetic susceptibility of a magnetically isolated U^V center with the same crystal field as **3**. The resulting effective spin coupling constants are $\hat{J}_{\parallel} = -66\ cm^{-1}$ and $\hat{J}_{\perp} = -7.7\ cm^{-1}$, which implies that the magnetic anisotropy, $g_{\perp}/g_{\parallel}$, of the U^V center in **3** is 0.34. The value of $\hat{J}_{\parallel}$ is the largest reported for a U^V complex, while a larger value of T_N has been observed in a U^{III} inverse sandwich complex, fitting the magnetic susceptibility of that complex to determine the coupling constant has not been possible.

ASSOCIATED CONTENT

Supporting graphics, experimental conditions, synthetic procedures, and spectroscopic data accompanies this paper. This material is available free of charge *via* the Internet at http://pubs.acs.org.

AUTHOR INFORMATION

Corresponding Authors

E-mail: karsten.meyer@fau.de.

E-mail: wwlukens@lbl.gov

Funding Sources

The Bundesministerium für Bildung und Forschung (BMBF 2020+, 02NUK012B), the FAU Erlangen-Nürnberg, and COST

Action CM1006. Portions of this work were supported by U.S. Department of Energy, Basic Energy Sciences, Chemical Sciences, Biosciences, and Geosciences Division and were performed at Lawrence Berkeley National Laboratory under Contract No. DE-AC02-05CH11231.

Notes

Supplementary information accompanies this paper at http://pubs.acs.org. Reprints and permission information is available online at http://pubs.acs.org. Correspondence and requests for materials should be addressed to W.W.L.jr. and K.M..

Competing financial interests

The authors declare no competing financial interests.

ACKNOWLEDGEMENTS

We thank Dr. A. K. Abdul-Sada and Prof. F. Geoffrey N. Cloke for performing mass spectrometry experiments. Furthermore, we gratefully acknowledge Prof. Dr. Dirk M. Guldi for use of his Raman spectrometer, and Dipl. Chem. Tobias Engesser and Prof. Dr. Ingo Krossing for kindly providing $Ag[Al(OC(CF_3)_3)_4]$ and $NO[Al(OC(CF_3)_3)_4]$.

REFERENCES

(1) Zhang, Z.; Pitzer, R. M. *J. Phys. Chem. A* **1999**, *34*, 6880-6886.
(2) (a) Burns, C. J.; Eisen, M. S., *The Chemistry of the Actinide and Transactinide Elements* 3rd ed.; Springer: Dodrecht, The Netherlands: 2006; Vol. 5. (b) Zalkin, A.; Beshouri, S. M. *Acta Crystallogr. C* **1988**, *10*, 1826-1827. (c) Zi, G.; Jia, L.; Werkema, E. L.; Walter, M. D.; Gottfriedsen, J. P.; Andersen, R. A. *Organometallics* **2005**, *17*, 4251-4264. (d) Arney, D. S. J.; Burns, C. J. *J. Am. Chem. Soc.* **1993**, *21*, 9840-9841. (e) Fortier, S.; Kaltsoyannis, N.; Wu, G.; Hayton, T. W. *J. Am. Chem. Soc.* **2011**, *36*, 14224-14227. (f) Fortier, S.; Brown, J. L.; Kaltsoyannis, N.; Wu, G.; Hayton, T. W. *Inorg. Chem.* **2012**, *3*, 1625-1633. (g) Lam, O. P.; Heinemann, F. W.; Meyer, K. *Chem. Sci.* **2011**, *8*, 1538-1547. (h) Arney, D. S. J.; Burns, C. J. *J. Am. Chem. Soc.* **1995**, *37*, 9448-9460. (i) de Wet, J. F.; du Preez, J. G. H. *J. Chem. Soc., Dalton Trans.* **1978**, *6*, 592-597. (j) Kosog, B.; La Pierre, H. S.; Heinemann, F. W.; Liddle, S. T.; Meyer, K. *J. Am. Chem. Soc.* **2012**, *11*, 5284-5289. (k) Mills, D. P.; Cooper, O. J.; Tuna, F.; McInnes, E. J. L.; Davies, E. S.; McMaster, J.; Moro, F.; Lewis, W.; Blake, A. J.; Liddle, S. T. *J. Am. Chem. Soc.* **2012**, *24*, 10047-10054. (l) Lewis, A. J.; Carroll, P. J.; Schelter, E. J. *J. Am. Chem. Soc.* **2013**, *35*, 13185-13192. (m) Lewis, A. J.; Carroll, P. J.; Schelter, E. J. *J. Am. Chem. Soc.* **2012**, *1*, 511-518.
(3) Jones, G. M.; Arnold, P. L.; Love, J. B. *Angew. Chem. Int. Ed.* **2012**, *50*, 12584-12587.
(4) Labouille, S.; Clavaguéra, C.; Nief, F. *Organometallics* **2012**, *5*, 1265-1271.
(5) (a) Lukens, W. W.; Edelstein, N. M.; Magnani, N.; Hayton, T. W.; Fortier, S.; Seaman, L. A. *J. Am. Chem. Soc.* **2013**, *29*, 10742-10754. (b) Roger, M.; Belkhiri, L.; Arliguie, T.; Thuery, P.; Boucekkine, A.; Ephritikhine, M. *Organometallics* **2008**, *1*, 33-42. (c) Camp, C.; Antunes, M. A.; Garcia, G.; Ciofini, I.; Santos, I. C.; Pecaut, J.; Almeida, M.; Marcalo, J.; Mazzanti, M. *Chem. Sci.* **2014**, *2*, 841-846. (d) Minasian, S. G.; Krinsky, J. L.; Arnold, J. *Chem. Eur. J.* **2011**, *44*, 12234-12245.
(6) (a) Chatelain, L.; Mougel, V.; Pecaut, J.; Mazzanti, M. *Chem. Sci.* **2012**, *4*, 1075-1079. (b) Mougel, V.; Horeglad, P.; Nocton, G.; Pécaut, J.; Mazzanti, M. *Angew. Chem. Int. Ed.* **2009**, *45*, 8477-8480. (c) Nocton, G. g.; Horeglad, P.; Pécaut, J.; Mazzanti, M. *J. Am. Chem. Soc.* **2008**, *49*, 16633-16645. (d) Spencer, L. P.; Schelter, E. J.; Yang, P.; Gdula, R. L.; Scott, B. L.; Thompson, J. D.; Kiplinger, J. L.; Batista, E. R.; Boncella, J. M. *Angew. Chem. Int. Ed.* **2009**, *21*, 3795-3798. (e) Rosen, R. K.; Andersen, R. A.; Edelstein, N. M. *J. Am. Chem. Soc.* **1990**, *11*, 4588-4590. (f) Arnold, P. L.; Jones, G. M.; Odoh, S. O.; Schreckenbach, G.; Magnani, N.; Love, J. B. *Nature Chem.* **2012**, *3*, 221-227. (g) Korobkov, I.; Gambarotta, S.; Yap, G. P. A. *Angew. Chem. Int. Ed.* **2002**, *18*, 3433-3436. (h) Rinehart, J. D.; Harris, T. D.; Kozimor, S. A.; Bartlett, B. M.; Long, J. R. *Inorg. Chem.* **2009**, *8*, 3382-3395. (i) Diaconescu, P. L.; Arnold, P. L.; Baker, T. A.; Mindiola, D. J.; Cummins, C. C. *J. Am. Chem. Soc.* **2000**, *25*, 6108-6109.
(7) Umetsu, R. Y.; Okamoto, Y.; Miyakawa, M.; Sasao, K.; Fukamichi, K.; Sakuma, A. *J. Magn. Magn. Mater.* **2004**, *0*, 790-791.
(8) Figgis, B. N.; Martin, R. L. *J. Am. Chem. Soc.* **1956**, *0*, 3837-3846.
(9) Vlaisavljevich, B.; Diaconescu, P. L.; Lukens, W. L.; Gagliardi, L.; Cummins, C. C. *Organometallics* **2013**, *5*, 1341-1352.
(10) Schmidt, A.-C.; Nizovtsev, A. V.; Scheurer, A.; Heinemann, F. W.; Meyer, K. *Chem. Commun.* **2012**, *69*, 8634-8636.
(11) Brown, J. L.; Fortier, S.; Lewis, R. A.; Wu, G.; Hayton, T. W. *J. Am. Chem. Soc.* **2012**, *37*, 15468-15475.
(12) (a) Hazra, S.; Majumder, S.; Fleck, M.; Mohanta, S. *Polyhedron* **2008**, *5*, 1408-1414. (b) Duval, P. B.; Burns, C. J.; Buschmann, W. E.; Clark, D. L.; Morris, D. E.; Scott, B. L. *Inorg. Chem.* **2001**, *22*, 5491-5496. (c) Spencer, L. P.; Yang, P.; Scott, B. L.; Batista, E. R.; Boncella, J. M. *Inorg. Chem.* **2009**, *24*, 11615-11623. (d) Wahu, S.; Berthet, J.-C.; Thuéry, P.; Guillaumont, D.; Ephritikhine, M.; Guillot, R.; Cote, G.; Bresson, C. *Eur. J. Inorg. Chem.* **2012**, *23*, 3747-3763.
(13) Bart, S. C.; Anthon, C.; Heinemann, F. W.; Bill, E.; Edelstein, N. M.; Meyer, K. *J. Am. Chem. Soc.* **2008**, *37*, 12536-12546.
(14) Lam, O. P.; Heinemann, F. W.; Meyer, K. *C. R. Chim.* **2010**, *6–7*, 803-811.
(15) La Pierre, H. S.; Meyer, K. *Inorg. Chem.* **2012**, *2*, 529-539.
(16) Castro-Rodriguez, I.; Olsen, K.; Gantzel, P.; Meyer, K. *Chem. Commun.* **2002**, *23*, 2764-2765.
(17) Graves, C. R.; Yang, P.; Kozimor, S. A.; Vaughn, A. E.; Clark, D. L.; Conradson, S. D.; Schelter, E. J.; Scott, B. L.; Thompson, J. D.; Hay, P. J.; Morris, D. E.; Kiplinger, J. L. *J. Am. Chem. Soc.* **2008**, *15*, 5272-5285.
(18) (a) Richardson, D. E.; Taube, H. *Inorg. Chem.* **1981**, *4*, 1278-1285. (b) Fox, A. R.; Arnold, P. L.; Cummins, C. C. *J. Am. Chem. Soc.* **2010**, *10*, 3250-3251.
(19) Guokui, L.; Beitz, J. V., *The Chemistry of the Actinide and Transactinide Elements* 3rd ed.; Springer: Dodrecht, The Netherlands: 2006; Vol. 5.
(20) (a) Mizuoka, K.; Tsushima, S.; Hasegawa, M.; Hoshi, T.; Ikeda, Y. *Inorg. Chem.* **2005**, *18*, 6211-6218. (b) Nocton, G.; Horeglad, P.; Vetere, V.; Pécaut, J.; Dubois, L.; Maldivi, P.; Edelstein, N. M.; Mazzanti, M. *J. Am. Chem. Soc.* **2009**, *2*, 495-508.
(21) Ryan, J. L. *J. Inorg. Nucl. Chem.* **1971**, *1*, 153-177.
(22) Selbin, J.; Sherrill, H. J. *Inorg. Chem.* **1974**, *5*, 1235-1239.
(23) Fortier, S.; Wu, G.; Hayton, T. W. *Inorg. Chem.* **2008**, *11*, 4752-4761.

(24) Graves, C. R.; Vaughn, A. E.; Schelter, E. J.; Scott, B. L.; Thompson, J. D.; Morris, D. E.; Kiplinger, J. L. *Inorg. Chem.* **2008**, *24*, 11879-11891.
(25) Thomson, R. K.; Scott, B. L.; Morris, D. E.; Kiplinger, J. L. *C. R. Chim.* **2010**, *6–7*, 790-802.
(26) Lever, A. B. P., *Inorganic electronic spectroscopy*. Elsevier Applied Science, AmsterdamNew York: 1984; Vol. 2.
(27) Kraft, S. J.; Williams, U. J.; Daly, S. R.; J. Schelter, E.; Kozimor, S. A.; Boland, K. S.; Kikkawa, J. M.; Forrest, W. P.; Christensen, C. N.; Schwarz, D. E.; Fanwick, P. E.; Clark, D. L.; Conradson, S. D.; Bart, S. C. *Inorg. Chem.* **2011**, *20*, 9838-9848.
(28) (a) Cooper, S. R.; Calvin, M. *J. Am. Chem. Soc.* **1977**, *20*, 6623-6630. (b) Larsen, P. L.; Parolin, T. J.; Powell, D. R.; Hendrich, M. P.; Borovik, A. S. *Angew. Chem. Int. Ed.* **2003**, *1*, 85-89. (c) Galas, A. R.; Hursthouse, M.; Behrman, E. J.; Midden, W. R.; Green, G.; Griffith, W. *Transition Met. Chem.* **1981**, *3*, 194-195.
(29) (a) Aboelella, N. W.; Lewis, E. A.; Reynolds, A. M.; Brennessel, W. W.; Cramer, C. J.; Tolman, W. B. *J. Am. Chem. Soc.* **2002**, *36*, 10660-10661. (b) Mahapatra, S.; Halfen, J. A.; Wilkinson, E. C.; Pan, G.; Wang, X.; Young, V. G.; Cramer, C. J.; Que, L.; Tolman, W. B. *J. Am. Chem. Soc.* **1996**, *46*, 11555-11574.
(30) (a) Dong, Y.; Fujii, H.; Hendrich, M. P.; Leising, R. A.; Pan, G.; Randall, C. R.; Wilkinson, E. C.; Zang, Y.; Que, L. *J. Am. Chem. Soc.* **1995**, *10*, 2778-2792. (b) Gamelin, D. R.; Kirk, M. L.; Stemmler, T. L.; Pal, S.; Armstrong, W. H.; Penner-Hahn, J. E.; Solomon, E. I. *J. Am. Chem. Soc.* **1994**, *6*, 2392-2399. (c) Schenker, R.; Mandimutsira, B. S.; Riordan, C. G.; Brunold, T. C. *J. Am. Chem. Soc.* **2002**, *46*, 13842-13855.
(31) (a) King, D. M.; Tuna, F.; McMaster, J.; Lewis, W.; Blake, A. J.; McInnes, E. J. L.; Liddle, S. T. *Angew. Chem. Int. Ed.* **2013**, *18*, 4921-4924. (b) Lewis, A. J.; Nakamaru-Ogiso, E.; Kikkawa, J. M.; Carroll, P. J.; Schelter, E. J. *Chem. Commun.* **2012**, *41*, 4977-4979.
(32) Kahn, O. *Angew. Chem. Int. Ed.* **1985**, *10*, 834-850.
(33) (a) Van Vleck, J. H., *The theory of electric and magnetic susceptibilities*. Clarendon Press: Oxford, 1932. (b) Gerloch, M., *Magnetism and Ligand-field Analysis*. Cambridge University Press: 1983.
(34) Stevens, K. W. H. *Proc. R. Soc. Lond. A* **1953**, *1139*, 542-555.
(35) Zuend, S. J.; Lam, O. P.; Heinemann, F. W.; Meyer, K. *Angew. Chem.* **2011**, 10814-10818.
(36) Flint, C. D.; Tanner, P. A. *Mol. Phys.* **1987**, *2*, 389-407.
(37) Siladke, N. A.; Meihaus, K. R.; Ziller, J. W.; Fang, M.; Furche, F.; Long, J. R.; Evans, W. J. *J. Am. Chem. Soc.* **2012**, *2*, 1243-1249.
(38) Lane, B. C.; Venanzi, L. M. *Inorg. Chim. Acta* **1969**, *0*, 239-245.
(39) Carretta, S.; Amoretti, G.; Santini, P.; Mougel, V.; Mazzanti, M.; Gambarelli, S.; Colineau, E.; Caciuffo, R. *J. Phys.: Condens. Matter* **2013**, *48*, 486001.
(40) Lukens, W. W.; Walter, M. D. *Inorg. Chem.* **2010**, *10*, 4458-4465.
(41) Costes, J.-P.; Dahan, F.; Dupuis, A.; Laurent, J.-P. *Chem. Eur. J.* **1998**, *9*, 1616-1620.
(42) Abragam, A.; Bleaney, B., *Electron paramagnetic resonance of transition ions*. Clarendon P.: 1970.
(43) Jones, J. E. R.; Hendricks, M. E.; Stone, J. A.; Karraker, D. G. *J. Chem. Phys.* **1974**, *5*, 2088-2094.
(44) (a) Jones, W. M.; Gordon, J.; Long, E. A. *J. Chem. Phys.* **1952**, *4*, 695-699. (b) Vogt, O.; Mattenberger, K.; Löhle, J. *J. Magn. Magn. Mater.* **2001**, *2–3*, 199-212.